RSC Advances

This article can be cited before page numbers have been issued, to do this please use: N. Shasmal, P. K and B. Karmakar, *RSC Adv.*, 2015, DOI: 10.1039/C5RA15501K.

ROYAL SOCIETY OF CHEMISTRY

www.rsc.org/advances

View Article Online
DOI: 10.1039/C5RA15501K

Enhanced Photoluminescence Up and Downconversions of Sm^{3+} ions by Ag nanoparticles in Chloroborosilicate Glass Nanocomposites

Nilanjana Shasmal[a,b], Pradeep K[c], Basudeb Karmakar[a,*]

[a]*Glass Science and Technology Section, CSIR-Central Glass and Ceramic Research Institute, 196 Raja S C Mullick Road, Kolkata-700032, India*
[b]*Academy of Scientific and Innovative Research, Chenna-600113, India*
[c]*Cochin University of Science and Technology, Kerala-682022, India*

Abstract

Sm^{3+} doped Ag-chloroborosilicate glass nanocomposite has been synthesized in a dielectric glass matrix SiO_2-B_2O_3-Al_2O_3-K_2O-$BaCl_2$ (CBS) by a single-step melt-quenching technique involving selective thermochemical reduction by a reducing agent. The T_g has been found to be 630-633°C as obtained by dilatometry and differential scanning calorimetry. The colourless nanocomposite was heat treated according to a pre-designed heat treatment protocol. X-ray diffraction patterns show the emergence of nanocrystalline phases of $BaCl_2$ and Ag^0 after certain heat treatment. Study of microstructure of the crystallized samples by field emission scanning electron microscopy and transmission electron microscopy reveals the presence of polycrystalline phase of $BaCl_2$. Refractive index was found to be 1.5987 at 632.8 nm. UV-Vis absorption spectra shows absorption bands around 400 nm which arises due to the surface plasmon resonance of Ag nanoparticles (NPs). The band gets widened with increasing crystallization of the glass matrix. Photoluminescence spectra (λ_{ex} = 447nm) shows enhanced downconversion of frequency which varies with heat treatment duration. The extent of enhancement was found to be dependent on the size of Ag NPs. Also the effect of matrix crystallization on the emission intensity is evident. Enhanced frequency upconversion (λ_{ex} = 949 nm) was found to take place only when the matrix becomes crystallized. This has happened due to the formation of low-phonon energy $BaCl_2$ nanocrystals and thereby decreasing of the non-radiative emission probabilities. These optical properties make the nanocomposite potential for various nanophotonic applications.

Keywords: Glass nanocomposites, melt-quenching technique, transmission electron microscopy, UV-Vis absorption, frequency upconversion

View Article Online
DOI: 10.1039/C5RA15501K

1. Introduction

Rare earth (RE) ions doped glasses, have been widely used for the development of many optoelectronic devices such as lasers, light converters, sensors, hole burning high-density memories, optical fibers and optical amplifiers.[1-3] The excitations and emissions of them are due to the transitions from the $4f^n$ electronic states of trivalent RE ions, which are highly sensitive to the symmetry, structure of the local environment and phonon energy of the host matrix.[3–6] Among the RE ions Sm^{3+} ions have motivated extensive interests due to their potential application for high-density optical memory devices, under sea communication and colour displays. [7-9] The excited $^4G_{5/2}$ level of Sm^{3+} ions emits in the visible region which exhibits relatively high quantum efficiency and shows different quenching mechanisms which make Sm^{3+} ions as an interesting case to analyze the energy transfer process.[10]

Consequently, there has been an exponential interest to enhance the efficiencies of these RE-doped optical materials. Recently, coupling of RE ions with metal nanoclusters has been developed as a valuable strategy to improve the luminescence efficiency of RE ions. These materials with enhanced luminescence properties, particularly nano metal enhanced upconversion and downconversion, are promising for plasmon controlled nano-photonic technologies.[11,12] Metal nanoparticles (NPs) can influence the photoluminescence emission of RE^{3+} ions in several ways. Local field enhancement induced by surface plasmon resonance (SPR) of metal NPs has often been accentuated as the potential cause of fluorescence enhancement when the excitation or emission is resonant or near the surface plasmon resonance (SPR) wavelength of metallic NPs.[13-16]

The surface plasmon resonance of noble metal NPs (gold and silver) is a remarkable phenomenon that already has cultivated many new powerful analytical techniques and applications. The collective oscillation of the noble metal valence electrons resonantly excited by visible light, the surface plasmon resonance (SPR), causes a tremendous enhancement of the electromagnetic near-field in the immediate vicinity of the particles. Characteristic enhancement factors of the electric field E are in the range of 10^2.[17,18]

Anisotropic nanoparticles with sharp edges (ellipsoids, nano-rods, etc.) are more potential candidates for plasmon enhanced fluorescence studies.[12,19] Upon electromagnetic excitation the local surface charge densities are drastically increased and confined near the sharp edges of anisotropic nanostructures which act as light-harvesting nano optical antennas converting visible light into large localized electric field (‘‘lightning-rod effect’’).[20] Inorganic

View Article Online
DOI: 10.1039/C5RA15501K

glasses have been proven as very suitable materials to stabilize gold and silver nanoparticles and to investigate their diverse optical properties.[21,22]

Sm^{3+} ion have been incorporated in several different glass systems. Spectroscopic and lasing characteristics of Sm^{3+} doped silicate glass fibres were first described by Farries et. al. in 1988. They showed that in silica glass Sm^{3+} shows fluorescence at a wavelength of 650 nm.[23,24] Effect of host glass composition on the optical absorption spectra of Sm^{3+} in lead borate glasses has been analyzed by Saisudha et. al.[25] Absorption and emission spectral studies of Sm^{3+} ion in PbO-PbF_2 oxyfluoride glass matrix were reported by Nachimuthu et. al.[26] Optical absorption spectra for Sm^{3+} ions in zinc and alkali zinc borosulphate glasses were presented by Jayasankar et. al.[27] Optical properties of Sm^{3+} doped oxyfluoroborate glass have been studied by Mahato et. al.[28] The absorption spectral studies have been performed for various rare earth ions (including Sm^{3+}) doped phosphate glass, $Na_4AlZnP_3O_{12}$.[29] Study of emission, absorption and vibrational properties of Sm^{3+} doped lead fluoroborate glasses as a function of the Sm^{3+} content were presented by Filho et. al. They present a wide range of transmission, which provides the observation of several absorption lines associated to the trivalent rare-earth ion (Sm^{3+}).[30] Sm^{3+}-doped cadmium–aluminum–silicate glasses have been fabricated and characterized optically. Intense visible lights and near-infrared emissions were observed under ultraviolet light and 488 nm laser excitation.[31] Sm^{3+} ions have also been doped in tellurite glass. Stark splitting has been observed in the upper and lower levels in fluorescence.[32] Sm^{3+}-doped rare-earth borate glasses having composition Li_2O–BaO–La_2O_3–B_2O_3 have been fabricated and characterized optically by Lin et. al.[33] Sm^{3+} has also been doped into the glass system B_2O_3–ZnO–PbO.[34] Optical absorption, luminescence and lifetime measurements of Sm^{3+}-doped alkali fluorophosphates and zinc–phosphate glasses have been described.[35,36]

Most oxide glasses have large phonon energy (1100 cm^{-1}) due to the stretching vibration of network-forming oxides Since many fluorescent transitions of rare-earth ions of practical importance are initiated from an excited level with a small energy gap, materials with lower phonon energy are often required as a luminescent host to suppress the non-radiative loss and to obtain higher quantum efficiency of the desired fluorescence.[37] Recently a low phonon glass system having composition SiO_2-B_2O_3-BaO-K_2O-Al_2O_3-$BaCl_2$ was reported[38] and luminescent properties of in situ generated Ag NPs within this system were also studied.[39] Here we have co-doped this chloroborosilicate glass system with Sm^{3+} and Ag to observe the optical properties of Sm^{3+}-doped low phonon glass in presence of Ag NPs. Thermal properties were studied by differential scanning calorimetry (DSC), and dilatometry.

View Article Online
DOI: 10.1039/C5RA15501K

Physical properties and microstructures were investigated by X-ray diffraction and field emission scanning electron microscopy (FESEM), transmission electron microscopy respectively. Optical properties were explored by refractive index measurement and optical spectroscopy. Enhancement has been found both in case of downconversion (when excited at 447 nm) and upconversion (when excited at 980 nm).

2. Experimental Procedure

2.1 Preparation

Chloroborosilicate glass (CBS) having composition $36.75SiO_2$-$26.25B_2O_3$-$20BaO$-$3.5K_2O$-$3.5Al_2O_3$-$12.5BaCl_2$ (mol%) in addition with 0.05 wt% $SnCl_2$ (in excess) was prepared by melt quench technique using quartz, SiO_2 (GR, Bremthaler, Quarzitwerk, Usinger. Germany), boric Acid, H_3BO_3 (GR, 99%, Loba Chemie, Mumbai, India), barium carbonate, $BaCO_3$ (GR, 99%, Fluka Chemie GmbH, Buchs, Switzerland), potassium carbonate, K_2CO_3 (GR, 99%, Loba Chemie, Mumbai, India), aluminium oxide, Al_2O_3 (GR, Aldrich Chemical Company Inc, Milwaukee 53233, USA) and barium chloride, $BaCl_2.2H_2O$ (GR, Dihydrated extra pure Loba Chemie, Mumbai, India) as the raw materials. They were used directly without any further purification. 100 g of glass was prepared by melting the well-mixed batches of calculated composition in a high-purity alumina crucible at 1400°C for 1.5 h with intermittent stirring for 0.5 min in air in a raising hearth electric furnace. The molten sample was cast into an iron plate in air and annealed at 550°C for 1 h in order to remove the residual thermal stresses, followed by a slow cooling down to room temperature. Three more glasses of same composition were prepared with addition of (i) 0.3 wt% Sm_2O_3 (GR, 99%, Loba Chemie, Mumbai, India), (ii) 0.3 wt% Sm_2O_3 and 0.1 wt% AgCl (GR, 99%, Loba Chemie, Mumbai, India) and (iii) 0.1 wt% AgCl in excess was prepared using the same procedure and annealed at 550°C using the same schedule. The monolithic glasses thus obtained were cut and polished into the desired shapes and sizes required for the different characterizations, as described below.

View Article Online
DOI: 10.1039/C5RA15501K

2.2 Characterization

The densities (ρ) of the glass samples were determined by the standard Archimedes principle. The measurements were done using single pan balance and distilled water as an immersion liquid. The density was obtained from the relation.

$$\rho = a\,\rho_x / (a-b) \quad (1)$$

Where *a* is the weight of the glass sample in air, *b* is the weight of the glass sample when suspended in distilled water (density of water, ρ_x = 0.997604 g·cm^{-3} at 25^{o}C). Differential scanning calorimetric experiment was performed by a differential scanning calorimeter (NETZSCH Model STA 449 Jupiter F3, NETZSCH-Gerätebau GmbH, Selb, Germany) taking powdered sample within the temperature range of 30^o-900^{o}C in nitrogen atmosphere at the heating rate of 10 K/min. The coefficient of thermal expansion (CTE, α), glass transition temperature (T_g), and dilatometric deformation temperature (T_d) was measured using a horizontal vitreous silica dilatometer (DIL 402C, Netzch-Gerä tebau GmbH, Bavaria, Germany) with a heating rate of 4 K/min taking a cylindrical sample of approximately 25 mm length and 5 mm diameter and heating it at a rate of 4 K/min up to the temperature where the glass softens, after calibration with a standard alumina supplied with the instrument by the manufacturer. The CTE values reported here are in the temperature range 50–150 °C. The CTE, Tg and Td values were reproducible with ±1 ºC for all samples. The X-ray diffraction (XRD) patterns of the bulk samples were recorded in an X'pert Pro MPD diffractometer (PANalytical, Almelo, the Netherlands), operating at 40 kV and 30 mA, using Ni-filtered CuKα radiation with the X'celerator, with a step size of 0.05º(2θ) and a step time of 0.5s, from 10º to 80º. The UV-Vis absorption spectra and the PL spectra of the all the samples were studied using polished 2 mm thick samples with the help of fiber optic spectrometer (AvaSpec-3648-USB2, Avantes) and diode lasers source of wavelength 447 and 949 nm.

3. Results and Discussion

The compositions and some physical properties of the glasses having general composition 36.75SiO_2-26.25B_2O_3-20BaO-3.5K_2O-3.5Al_2O_3-12.5$BaCl_2$ (mol%) are listed in Table 1. All samples are obtained as colourless and transparent monoliths. Figure 1 shows the

View Article Online
DOI: 10.1039/C5RA15501K

photographs of the prepared samples and EDX spectrum of sample CBS3 showing the inclusion of $BaCl_2$ into the glass.

3.1 Density

The densities of the glasses and nanocomposites are found to be in the range of 3.3434 - 3.3597 $g.cm^{-3}$. The measured densities have been listed in Table 1. The densities of the samples are almost equal as there is a very little variation in their composition. Densities have been measured at different times and found unaltered after long exposure to air and moisture. Their densities do not change even after emerging it long time into water. This proves the glasses and the composites to be resistant to weather. Densities are measured after thermal treatment also and found to be unchanged even after long durations. This ensures the thermal stability of the samples.

3.2 Dilatometry and Differential Scanning Calorimetry

Glass transition temperature (T_g) and dilatometric softening point (T_d) of the nanocomposite CBS-3 were measured by dilatometric measurement taking a cylindrical sample of approximately 25 mm length and 5 mm diameter and heating it at a rate of 4K/min up to the temperature where the glass softens. Figure 2(a) shows the dilatometric curve of the glass. T_g and T_d was found at around 633º and 672ºC respectively.

Differential scanning calorimetry (DSC) was also performed to determine the T_g and thermal behaviour of the glass taking finely grinded powder of the composite CBS-3 and heating it at the rate of 10K/min from 30-900^{0}C. The DSC thermogram has been shown in Fig 2(b). T_g was found at about 630ºC. The T_g determined by dilatometry and DSC are almost similar.

3.3 Heat Treatment and physical appearance

To develop metallic nanoparticles into the glass matrix, all the four samples were undergone thermal treatment following a carefully designed heat treatment schedule. The temperature of heat treatment was determined from the dilatometric and DSC thermograms. The temperature should be such selected that atomic rearrangements and diffusion process can take place without deforming the glass structure. From the definition of T_g it is known that above T_g the chain segments can slip pass one another i.e. molecular movement can take place. And T_d is the temperature where the glass structure starts to deform. So the optimum

View Article Online
DOI: 10.1039/C5RA15501K

temperature, at which development of metallic nanoparticles can take place smoothly, should be somewhere near the midpoint between T_g and T_d. Thus we selected 650°C for the heat treatment as it is approximately the midpoint between 633º and 672ºC. The samples were heat treated at 650°C for different durations- 15m, 30m, 1h, 2h, 3h, 5h and 8h. Fig 3 shows the photographs of the heat treated samples. As evident from the figure all the samples of CBS-1 and CBS-2 are transparent whereas 5h and 8h heat treated samples of CBS-3 and CBS-4 are translucent in nature. The reason is the crystallization of the glass matrix which takes place due to the presence of the nanometal.

3.3 Thermochemical reduction reaction

Here, in this synthesis process, the overall thermochemical reduction reaction is

$$Sn^{2+} + 2Ag^{+} \rightarrow 2Ag° + Sn^{4+} \quad (2)$$

The standard electrode potential (E°) for the redox couples (Sn^{4+}/Sn^{2+}) and ($Ag^{+}/Ag°$) are -0.384 V and 0.799 V, respectively. Using these values, the calculated electrode potential (E^{o}_{cell}) for the above reaction (Eq. 1) has been found to be 1.214 V with the help of Nernst equation.

$$E^{o}_{cell} = E^{o} - \frac{RT}{nF} \ln K_{eq} \quad (3)$$

The free energy associated with the above thermo-chemical reduction was calculated from the equation,

$$\Delta G^{o} = -nFE^{o} \quad (4)$$

where, F is the Faraday's constant and n is the number of electrons transferred in this process. The calculated $\Delta G°$ is found to be -234.2 kJ/mol. Hence the thermochemical reduction as shown in Eq. 1 is spontaneous.[39]

3.3 XRD

Figure 4(a) shows the XRD spectra of CBS-3 as prepared and heat treated at 650°C for different time durations. From the figure it is evident that up to 3h heat treatment there is no evidence of crystallization found. The small hump between 2θ = 20°-30° indicate the

View Article Online
DOI: 10.1039/C5RA15501K

amorphicity of the glasses. After 3 hours, sharp peaks are found to appear along with the hump, indicating the formation of crystalline phases into the glass matrix. Figure 4(b) shows the XRD spectrum of CBS-3 heat treated at 650°C for 8h. The peaks have been identified by corresponding JCPDS file numbers.

Prominent peaks have been found at 2θ = 20.42°, 23.7°, 24.67°, 27.42°, 29.103°, 34.46°, 37.4°, 39.93°, 39.78°, 44.76°, 57.3°, 61.3°. Peaks at 2θ = 20.42°, 39.78° and 23.7° are due to diffractions from (111), (311) and (200) planes respectively of cubic crystalline phases of $BaCl_2$ (JCPDS 70-1076). Peaks at 2θ = 24.67°, 27.42°, 39.13° and 61.3° are due to diffractions from (220), (211), (420), (002), (430) and (013) planes respectively of monoclinic crystalline phase of $BaCl_2$ (JCPDS 83-0786). Peak at 2θ = 34.46° is due to diffraction from (220) plane of cubic crystalline phases of $BaCl_2$ (JCPDS 24-0095). Peaks at 2θ = 29.103° and 57.3° are due to diffractions from (202) and (413) planes respectively of tetragonal crystalline phase of Ba_3OSiO_4 (JCPDS 70-0667). Peaks at 2θ =37.24° and 44.53° are due to diffractions from (111) and (200) planes respectively of cubic crystalline phases of Ag^0 (JCPDS 4-0783).[38,39]

3.4 Field Emission Scanning Electron Microscopy

Figure 5 (a) and (b) are the FESEM micrographs of CBS-1 heat treated at 650°C for 5h and Fig 5 (c) and (d) are that of CBS-3 heat treated at 650°C for 5h. From the micrograph it is evident that both the heat treated samples are well crystallized. In CBS-1 it has been found that small crystals having diameter in the range 20-50 nm are in agglomerated form. The agglomerations have different range of sizes in different parts. Somewhere they are small spheres having diameter around 300-500 nm and somewhere many spherical agglomerates are associated together to form a cloud-like crystalline zone, as evident in Fig 5 (b). Most of the crystals and agglomerates are spherical in shape. Most of the individual crystals are in agglomerated form. A very few of them are found separate and their size is around 10-20 nm. The picture is a bit different in CBS-3. Here the agglomerates are much smaller in size, in the range 70-100 nm, as clear from fig 5 (c). A considerable number of individual crystals are found which are not agglomerated. And also the size of the agglomerates is more homogeneous than that of CBS-1. In fig 5(d) a big agglomerate is shown where individual

View Article Online
DOI: 10.1039/C5RA15501K

crystals and agglomerates are clearly visible and they are perfectly spherical in shape. This difference of microstructure is due to the effect of nanometal. Nanometals have the tendency to accelerate the crystallization process, which is also evident from the physical appearance of the heat treated samples. Nanometals control both the shapes and sizes of the individual crystals and the agglomerates and also their distribution in the glass matrix.

3.5 Transmission Electron Microscopy

Figure 6 (a) is a representative TEM micrograph of CBS-3 heat treated at 650°C for 5 hr. The nanocrystalline particles are clearly visible here. There are several particles having size in the range 5-25 nm. As confirmed from XRD results, this heat treated sample contains nanocrystalline phases of $BaCl_2$, Ba_3OSiO_4 and Ag. Thus we may say the observed particles are $BaCl_2$, Ba_3OSiO_4 and Ag nanoparticles, randomly distributed over the glass matrix. Like the FESEM micrographs, the nanoparticles observed here are almost spherical in shape. Figure 6 (b) shows the Selected Area Electron Diffraction (SAED) pattern of the same sample. The pattern clearly proves the presence of crystalline phases in the glass matrix. The appearance of multiple rings indicates the presence of multiple polycrystals. The patterns have been identified and matched with respective d-spacing values of the component. Starting from the centre the first ring is due to the diffraction from (111) plane of $BaCl_2$ (JCPDS 70-1076), second one is from (224) plane of Ba_3OSiO_4 (JCPDS 70-0667), third one is from (220) plane of $BaCl_2$ (JCPDS 83-0786). The fourth, fifth and sixth rings are due to the diffractions from (211) plane of $BaCl_2$ (JCPDS 83-0786), (211) plane of $BaCl_2$ (JCPDS 70-1076) and (311) plane of $BaCl_2$ (JCPDS 70-1076) respectively.

3.6 Refractive Index

Refractive index (n_i) at different wavelengths was measured for all the transparent glasses by Prism coupler using lasers of five different wavelengths. Figure 7 shows the variation of refractive index of different glasses with respect to the wavelength. Refractive indices are in the range 1.6030–1.6061 for 532 nm wavelength. It is evident that the value of n_i does not show noticeable change as there is a very slight variation of composition of the

View Article Online
DOI: 10.1039/C5RA15501K

samples and their densities are almost similar. The n_i of a particular medium is the ratio of velocity of light through the vacuum (c) to the velocity of light through the medium (v).

$$n_i = {}^{c}/_{v} \quad (5)$$

As all the samples are almost equally dense, the velocities if light through them are nearly equal, which leads to almost no variation in n_i values. The refractive indexes of the heat treated samples were also measured using the same technique. As the density remains unaltered with heat treatment, refractive index also does not change.

3.7 UV-Vis absorption

Figure 8(a) and (b) shows the UV-Vis absorption spectra of CBS-2 and CBS-3, respectively, heat treated at 650°C for different durations. From fig 8(a) it is clear that all the heat treated glasses are transparent both in the visible and NIR range. With increasing heat treatment duration the spectra do not show much significant change in their position and pattern. A prominent absorption band has been found at around 405 nm for all the samples. The appearance of this band may be attributed to the spectral transition ${}^{6}H_{5/2}$ to ${}^{6}P_{3/2}$ of Sm^{3+} ion. Another small band appears at around 1080 nm which is due to another transition ${}^{6}H_{5/2}$ to ${}^{6}F_{9/2}$.[40] The nature of the spectra for CBS-3 glasses is different. Up to 2h heat treatment duration they do not show any significant variation. But after that, from 3h heat treated sample, a totally different pattern has been observed. For 3, 5 and 8 h heat treated samples, a large band has been obtained which is spread around 300-450 nm.

Coinage metal (e.g. Ag, Au, Cu etc) NPs exhibit a potential resonant absorption and scattering of the electromagnetic light wave in the visible region which is the result of the collective coherent oscillation of the conduction electron gas of metal NPs. This is called local surface plasmon resonance (LSPR). It is known that silver NPs doped soda–lime silicate glasses exhibits plasmon peak of Ag NPs at around 410 nm.[40] Hence, the widespread band around 410 nm, associated with the absorption band of heat-treated samples, is clearly due to the surface plasmon resonance (SPR) absorption of Ag NPs. It is also evident from the spectra (figure 8 (b)) that both the intensity and broadness of the plasmon band increases with increase in heat treatment duration (from 3h to 8h). This happens because two types of phenomena take place simultaneously as the heat treatment time increases. They are the

View Article Online
DOI: 10.1039/C5RA15501K

enlargement of existing Ag NPs size and at the same time, formation of new Ag NPs, which are generated through the spontaneous thermo-chemical reduction process as mentioned in Eq. 1. Up to 2 hours they show gradual broadening, but after that the absorption band becomes very widely broadened. This is due to the fact that the size distribution of Ag NPs becomes wider as the duration of heat treatment increases, keeping the position of the peak almost unaltered. At 650°C for longer durations, the extent of crystallization of the glass matrix becomes higher and larger crystallites are formed. This is supported by the XRD results, which show that, the crystallization phenomena begin to take place after 3h. As a result of this, scattering effect begins to take place.[41] Both the scattering from the large crystallites as well as the formation of new Ag NPs are responsible for the huge broadening of the absorption band.

The wide spectra obtained for 3, 5 and 8 hours duration, are combinations of some merged peaks. If they are deconvoluted, 3-4 merged peaks can be found. The multiple peaks indicate that the Ag NPs show multiple sharp molecular like transitions. In the electronic structure of Ag NP, the highest occupied molecular orbitals (HOMOs) and the lowest unoccupied molecular orbitals (LUMOs) are composed of *sp* and *d* bands which are formed by the linear combination of atomic orbitals of individual Ag atoms. The HOMO and LUMOs above the Fermi energy level are originated from the *sp* band. The multiple peaks arise due to different HOMO to LUMO transitions which can be intra band (e.g. *sp* to *sp*) or inter band (e.g. *d* to *sp*) type.[39]

3.8 Photoluminescence

Photoluminescence (PL) spectra have been taken for all the heat treated samples of CBS-2 and CBS-3 exciting them at 447 and 980 nm laser diode source. Enhanced frequency downconversion and upconversion have been obtained respectively.

3.8.1 Enhanced Frequency Downconversion

All the heat treated samples of CBS-2 and CBS-3 give orange emission spectra when excited by 447 nm laser diode source. Figure 9(a) shows the chromaticity diagram corresponding to the light emitted from CBS-3, heat treated at 650°C for 15m. The point P represents chromaticity coordinates (x = 0.606, y = 0.391) of the emitted light, which corresponds to orange colour. Figure 9(b) and (c) are the photographs of CBS-1 and CBS-3 respectively, both heat treated at 650°C for 15m. As the blank glass CBS-1 does not contain

View Article Online
DOI: 10.1039/C5RA15501K

any RE or NM, it does not show any kind of photoluminescence, as result we get the characteristic blue light of the laser source. But the sample CBS-3 contains both RE and NM. It clearly shows the orange light emission which is also in agreement with the color coordinates.

Figure 10 (a) and (b) show the photoluminescence spectra of CBS-2 and CBS-3 respectively, heat treated for different durations. The spectra have four prominent emission bands at 563, 601, 648, 708 nm. The band at 601 nm has the highest intensity and it corresponds to orange color. The insets represent magnified views of this band where variation of intensity with heat treatment time can be clearly seen. Figure 11 shows the Partial energy level diagram of Sm^{3+} ion and Ag NPs showing the energy transfer mechanisms for the major bands in the downconversion spectra. The bands at 563, 601, 648 and 708 nm corresponds to the transitions $^4G_{5/2} \longrightarrow {}^6H_{5/2}$ ($\Delta J = 0$, zero–zero band, forbidden transition), $^4G_{5/2} \longrightarrow {}^6H_{7/2}$ ($\Delta J = 1$, magnetic dipole transition), $^4G_{5/2} \longrightarrow {}^6H_{9/2}$ ($\Delta J = 2$, hypersensitive electric dipole transition) and $^4G_{5/2} \longrightarrow {}^6H_{11/2}$ ($\Delta J = 3$, forbidden transition) respectively.[22]

If the variation of PL intensities with heat treatment time is observed, it is evident that both CBS-2 and CBS-3 exhibit same trend of variation. Fig 12 shows the variation of PL intensities with respect to heat treatment time. The plot reveals that initially the PL intensity increases with increasing heat treatment duration up to a certain limit, which is 30m. After that it decreases up to 3 h followed by a considerable increment up to 8h. This kind of variation can be explained by the various changes in internal structure of the nanocomposites taking place with the increasing heat treatment duration. The initial increase of PL is due to the effect of Ag NPs. The as prepared glass also exhibits PL emission, which indicates that Ag NPs have already been formed into the glass during melting or annealing stages. With heat treatment both the size and number of NPs increase. The strong local electric field in the Ag NPs arising from the SPR excitations which leads to the enhancement of the electric fields of the incoming (exciting) and outgoing (emitting) photons by the excited NPs, is responsible for this increment in PL intensity.[42] But PL intensity cannot increase continuously with increasing size of the NPs. After further heat treatment PL intensity gradually decreases. When the size of NPs are too small as compared to the mean free path of the conduction electrons inside the particles, the collision of the conduction electrons with the surface of the NPs causes damping of the SPR excitations and PL intensity remains low. With heat treatment the particle size increases and consequently the damping effect decreases. As result the PL intensity increases gradually until the size of the NPs is lower than the value of

View Article Online
DOI: 10.1039/C5RA15501K

the mean free path. When the size of the NPs exceeds the value of mean free path, decrease in the PL intensity is observed due to radiative damping effect.[43]

The further increase after 3h is due to the effect of matrix crystallization. As confirmed from XRD patterns, the glass matrix starts to crystallize after 3 h heat treatment duration. Initially very small crystallites are formed having size in the range of nanometers. Formation of these nanocrystals lowers down the phonon energy of the glass system. From the peak assignment of the XRD plot we get sharp peaks of $BaCl_2$ in major amount. The glass containing these $BaCl_2$ nanocrystals within its matrix has phonon energy as low as $350cm^{-1}$.[38] Low phonon systems enhances the emission intensity of the RE ions by lowering the non-radiative loss. That is why the PL intensity increases with extent of crystallization.

If the two curves in fig 12 is compared it is evident that PL intensity of CBS-3 is higher than that of CBS-2 at every point. This enhancement is attributed to the presence of Ag NPs. CBS-2 and CBS-3 has the exactly same amount of RE ions and has been heat treated at similar conditions. So the difference in PL intensity can only arise from the NM content of CBS-3. Such PL intensification of the Sm^{3+} ion emission is primarily due to the local field enhancement (LFE) around the RE ions sites induced by SPR of Ag NPs.[22] The plasmonic Ag NPs concentrates the incident electromagnetic field creating an additional field in the sub wavelength structures around the Sm^{3+} ion sites and subsequently increase their rate of excitation (by ‘‘Lightning Rod Effect’’).[20,22]

The secondary reason for enhanced luminescence is that when the Sm^{3+} is present in close vicinity to the metal surface, the weak photoluminescence emissions from the Ag NPs is added as a second channel of excitation energy, that is, energy transfer (ET) from Ag^0 to Sm^{3+}.[22] Thus, the Ag NPs increases the photonic density around the Sm^{3+} ions situated in near vicinity and thereby increase the number of photons captured by the Sm^{3+} ions. As a result of superior excitation rate the population of the excited state of the Sm^{3+} ions increases and subsequently the rate of radiative decay increases.

3.8.2 Enhanced Frequency Upconversion

Figure 13(a) and (b) represents the upconversion spectra of CBS-2 and CBS-3 heat treated at 5 h and 8h respectively (excitement wavelength is 980 nm). In both the figures

View Article Online
DOI: 10.1039/C5RA15501K

three sharp peaks are observed at 631, 646 and 783 nm. The transitions associated with the peaks are $^4G_{5/2} \longrightarrow {}^6H_{9/2}$ ($\Delta J = 2$, hypersensitive electric dipole transition), $^4G_{5/2} \longrightarrow {}^6H_{11/2}$ ($\Delta J = 3$, forbidden transition), $^4G_{5/2} \longrightarrow {}^6F_{1/2}$ ($\Delta J = 2$, hypersensitive electric dipole transition) respectively. Figure 14 shows the partial energy level diagram of Sm^{3+} ion and Ag NPs showing the energy transfer mechanisms for the major bands in the upconversion spectra. Like the downconversion mechanism here also enhancement is observed. From the spectra it is evident that CBS-3 is showing near about 50 fold increase from CBS-2 in upconversion frequency both in 5h and 8h duration. And it is quite obvious that the reason behind this huge enhancement is the presence of Ag NPs in CBS-3. The Ag NPs boost the PL intensity by their local field enhancement (LFE) around the RE ions sites induced by their SPR, as well as the energy transfer (ET) from Ag^0 to Sm^{3+}, following the same enhancement mechanism for downconversion. But here the enhancement is much higher than that of the downconversion. The reason is the change of environment of the REs and NPs. It has been observed that samples heat treated for durations less than 5 h do not show any upconversion. As evident from the XRD results, after 5 h heat treatment the samples get well crystallized. And upconversion is taking place only when the glass matrix becomes crystallized. Crystallization in chloroborosilicate glass leads to the lowering of phonon energy of the system, from ~1100 cm^{-1} to ~350cm^{-1}. This low-phonon glass matrix enhances the PL intensity of the RE ion by reducing the non-radiative loss. The splitting of the peaks is also the effect of crystallization, which is known as Stark effect. Such splitting is not observed in the downconversion spectra. Thus it is evident that the upconversion phenomenon is the effect of matrix crystallization.

4. Conclusions

Chloroborosilicate glasses having composition 36.75SiO_2-26.25B_2O_3-20BaO-3.5K_2O-3.5Al_2O_3-12.5$BaCl_2$ (mol%) have been prepared and doped with Sm^{3+}. Ag NPs have been generated into the glass by electrochemical reduction method using $SnCl_2$ as the reducing agent. The glasses were heat treated at 650°C for different durations. The as prepared and heat treated samples were characterized. The following points can be concluded from this study.

- Both DSC and dilatometric study shows the nanocomposite (CBS-3) has T_g around 630°C.
- The electrochemical reduction reaction, used here for in-situ generation of Ag NPs, is a spontaneous reaction having negative $\Delta G°$ value.

View Article Online
DOI: 10.1039/C5RA15501K

- XRD shows the nanocomposite gets crystallized after 5h heat treatment duration. The crystallized matrix shows sharp peaks of $BaCl_2$, Ba_3OSiO_4 and Ag.
- FESEM shows the effect of nanometal on the crystallization of the matrix. TEM and SAED confirm the emergence of crystallized matrix with increasing heat treatment duration, which supports the XRD results.
- UV-Vis absorption spectra of CBS-2 show the characteristic absorption bands for Sm^{3+} and CBS-3 show the characteristic SPR band of Ag at around 410 nm. The SPR band becomes widespread when the matrix becomes crystallized.
- When excited at 447 nm, both CBS-2 and CBS-3 give intense orange emission. The downconversion spectra have sharp emission bands. PL intensity increases with heat treatment after 45 m and then decreases. This is controlled by the size of NPs. After 3h, PL intensity again increases. This is the effect of crystallized low-phonon glass matrix.
- When excited at 980 nm CBS-2 and CBS-3 exhibit frequency upconversion only for samples heat treated for 5 h or more. This is again the effect of matrix crystallization. The low-phonon environment reduces the non-radiative loss and thus intensifies the upconverted frequency. Around 50 fold increase has been observed in CBS-3 than that of CBS-2 due to the presence of Ag NPs.

Acknowledgements

The authors are thankful to Mr. Kamal Dasgupta, Acting Director of the institute and Dr. Ranjan Sen, Head, Glass Division for their encouragement and support. The authors acknowledge the technical supports provided by the X-ray and electron microscopy section of the institute. NS would like to express her sincere gratitude for the financial support of the Academy of Scientific and Innovative Research (AcSIR) and Council of Scientific and Industrial Research (CSIR). Partial financial support under CSIR-TAPSUN Project NWP0055 is also gratefully acknowledged.

View Article Online
DOI: 10.1039/C5RA15501K

References

1 A. Agnesi, P. Dallocchio, F. Pirzio, G. Reali, *Opt. Commun.,* 2009*,* **282**, 2070.

2 H. Kalaycioglu, H. Cankaya, G. Ozen, L. Ovecoglu, A. Sennaroglu, *Opt. Commun.,* 2008, **281,** 6056.

3 I. A. Rayappan, K. Selvaraju, K. Marimuthu, *Physica B*, 2011, **406,** 548–555

4 S. Schweizer, L.W. Hobbs, M. Secu, J. Spaeth, A. Edgar, G.V.M. Williams, *Appl. Phys. Lett.* 2003, **83,** 449.

5 M. Rami Reddy, S.B. Raju, N. Veeraiah, *J. Phys. Chem. Solids,* 2000, **61,** 1567.

6 Y.C. Ratnakaram, D. Thirupathi Naidu, A. Vijayakumar, N.O. Gopal, Physica B, 2005, **358,** 296.

7 M.Nogami, Y.Abe, K.Hirao, D.H.Cho, *Appl.Phys.Lett.,* 1995, **66**, 2952.

8 P.Mikhail, M.Schnieper, H.Bill, J.Hulliger, *Phys.Status Solidi B,* 1999, **215,** R17.

9 A.Kurita, T.Kushida, T.Izumitani, M.Matsukawa, Opt. Lett., 1994, **19,** 314.

10 S. S. Sundari, K. Marimuthu, M.Sivraman, S. S. Babu, *J. Lumin.,* 130 (2010) 1313–1319

11 P.N. Prasad, *Nanophotonics,* Wiley: New Jersey, 2004; pp 129–151.

12 T. Som, B. Karmakar, *J. Appl. Phys.,* 2009, **105**, 013102.

13 O.L. Malta, P.A. Santa-Cruz,; G.F. De Sa´, F Auzel, *J. Lumin.,* 1985, **33,** 261–272.

14 S.T. Selvan,; T. Hayakawa, M. Nogami, *J. Phys. Chem. B,* 1999, **103,** 7064–7068.

15 Z. Pan, A. Ueda,; R. Aga, Jr, A.Burger, R. Mu, S.H. Morgan, *J. Non-Cryst. Solids,* 2010, **356,** 1097–1101.

16 T. Som, B. Karmakar, J. Mod. Optic., 2011, **58,** 1012-1023,

17 M. Eichelbaum, K. Rademann, *Adv. Funct. Mater.,* 2009, **19,** 2045–2052

18 U. Kreibig, M. Vollmer, *Optical Properties of Metal Clusters,* Springer, Berlin 1995.

19 P.P. Pompa, L. Martiradonna, A. Della Torre, F. Della Sala, L. Manna, M. De Vittorio, F. Calabi, R. Cingolani, R. Rinaldi, *Nat. Nanotechnol.,* 2006, **1,** 126–130.

20 F. Le, D.W. Brandl, Y.A. Urzhumov, H. Wang, J. Kundu, N.J. Halas, J. Aizpurua, P. Nordlander, *ACS Nano,* 2008, 2, 707–718.

21 M. Eichelbaum, K. Rademann, R. Muller, M. Radtke, H. Riesemeier, W.Gorner, *Angew. Chem.,* 2005, **117,** 8118

22 T. Som, B. Karmakar, *Appl. Surf. Sci.,* 2009, **255,** 9447–9452

23 M.C Farries, P.R. Morkel, J.E. Townsend, *Electron. Letters,* 1988, **24,** 709-711

24 M.C Farries, P.R. Morkel, J.E. Townsend, *IEE Proceedings,* 1990, **137,** 318-322

25 M. B. Saisudha, J. Ramakrishna, *Phys. Rev. B,* 1996, **53,** 6186-6196

View Article Online
DOI: 10.1039/C5RA15501K

26 P. Nachimuthu, R. Jagannathan, V. Nirmal Kumar, D. Narayana Rao, J.Non-Cryst. Solids, 1997, **217,** 215-223

27 C.K. Jayasankar , E. Rukmini, *Opt. Mater.,* 1997, **8,** 193-205

28 K.K. Mahato, D.K. Rai and S.B. Rai, Solid State Commun., 1998, **108,** 671–676.

29 G. V. Prakash, *Mater. Lett.,* 2000, **46,** 15–20

30 A.G. S. Filho, J. M. Filho, F.E.A. Melo, M.C.C. Custodio, R. Lebullenger, A.C. Hernandes, *J.Phys. Chem. Solids,* 2000, **61,** 1535–1542

31 H. Lin, E. Y. B. Pun, L. H. Huang, X. R. Liu, *Appl. Phys. Lett.,* 2002, **80,** 2642-2644

32 A. Kumar, D.K. Rai, S.B. Rai, *Spectrochim. Acta A,* 2003, **59,** 917-925

33 H. Lin, D.Yang, G. Liu, T. Ma, B. Zhai, Q. An, J. Yu, X. Wang, X. Liu, E.Yue, B. Pun, *J. Lumin.,* 2005, **113,** 121–128

34 G. Lakshminarayana, S. Buddhudu, *Physica B.,* 2006, **373,** 100–106

35 M. Jayasimhadri, L.R. Moorthy, S.A. Saleem, R.V.S.S.N. Ravikumar, *Spectrochim. Acta A,* 2006, **64,** 939–944

36 B. Eraiah, Sudha G. Bhat, *J. Phys. Chem. Solids,* 2007, **68,** 581–585

37 G. Lakshminarayana, J. Qiu, *J.Alloy. Compd.,* 2009, **476,** 470–476

38 N. Shasmal, A. R. Molla, B. Karmakar, J.Non-Cryst. Solids, 2014, **398–399,** 32–41

39 N. Shasmal, B. Karmakar, *Plasmonics,* 2015, **10,** 191-202

40 K.L Kelly, E. Coronado, L.L Zhao and G.C Schaltz, J. Phys. Chem. B, 2003, **107,** 668-677

41 G. Mie, *Ann. Phys.,* 1908, **330,** 377–445.

42 J. Qiu, M. Shirai, T. Nakaya, J. Si, X. Jiang, C. Zhu, K. Hirao, *Appl. Phys. Lett.,* 2002, **81,** 3040

43 S. Link, A. Beeby, S. FitzGerald, M.A. El-Sayed, T. Schaaff, R.L. Whetten. *J. Phys. Chem. B,* 2002, **106,** 3410-3415

View Article Online
DOI: 10.1039/C5RA15501K

Table 1: Composition and some physical properties of the nanocomposites

Glass/Composite ID	Composition (wt%)			Colour	Form	Density($g.cm^{-3}$)	
	$SnCl_2$	Sm_2O_3	AgCl			As prepared	After 8h heat treatment
CBS-1	0.05	-	-	Colourless	Transparent monolith	3.3597	3.3596
CBS-2	0.05	0.3	-	Colourless	Transparent monolith	3.3490	3.3492
CBS-3	0.05	0.3	0.1	Colourless	Transparent monolith	3.3501	3.3500
CBS-4	0.05	-	0.1	Colourless	Transparent monolith	3.3434	3.3432

View Article Online
DOI: 10.1039/C5RA15501K

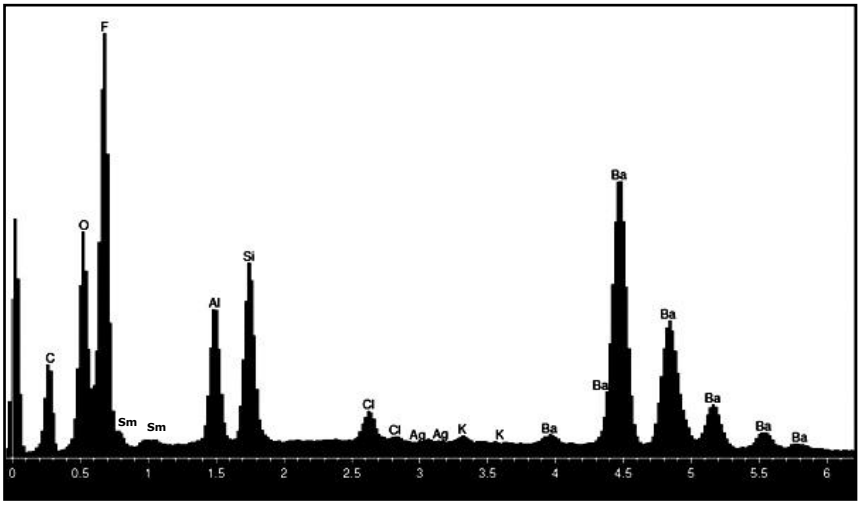

Fig 1. EDX spectrum of CBS-3 showing the presence of Ag and Sm in the glass matrix (See Table 1 for composition)

View Article Online
DOI: 10.1039/C5RA15501K

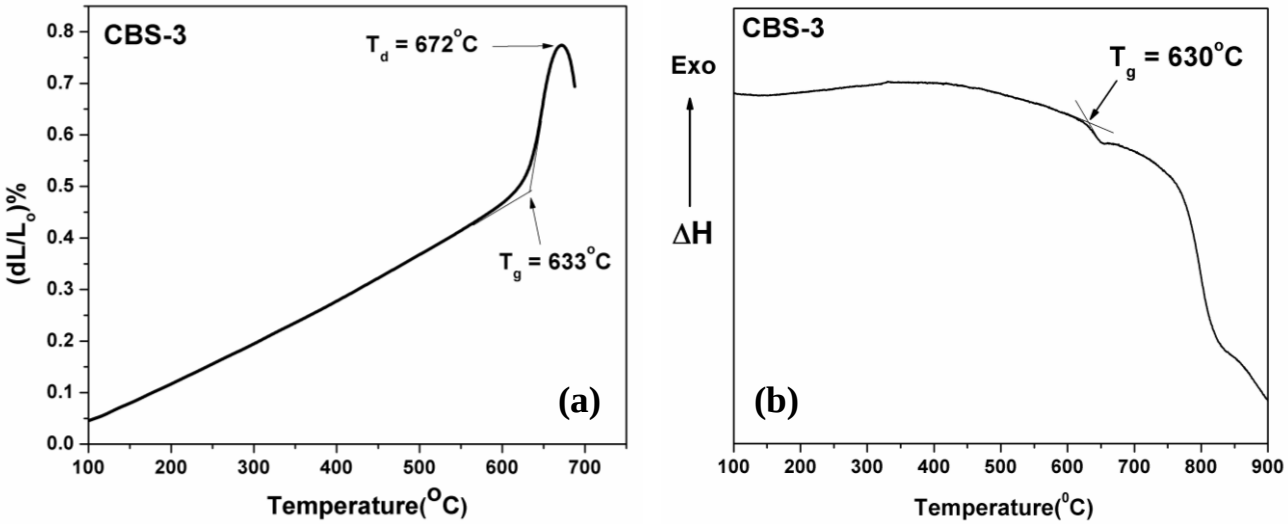

Fig 2. (a) Dilatometric thermogram and (b) differential scanning calorimetric curve of CBS-3 (See Table 1 for composition)

.

View Article Online
DOI: 10.1039/C5RA15501K

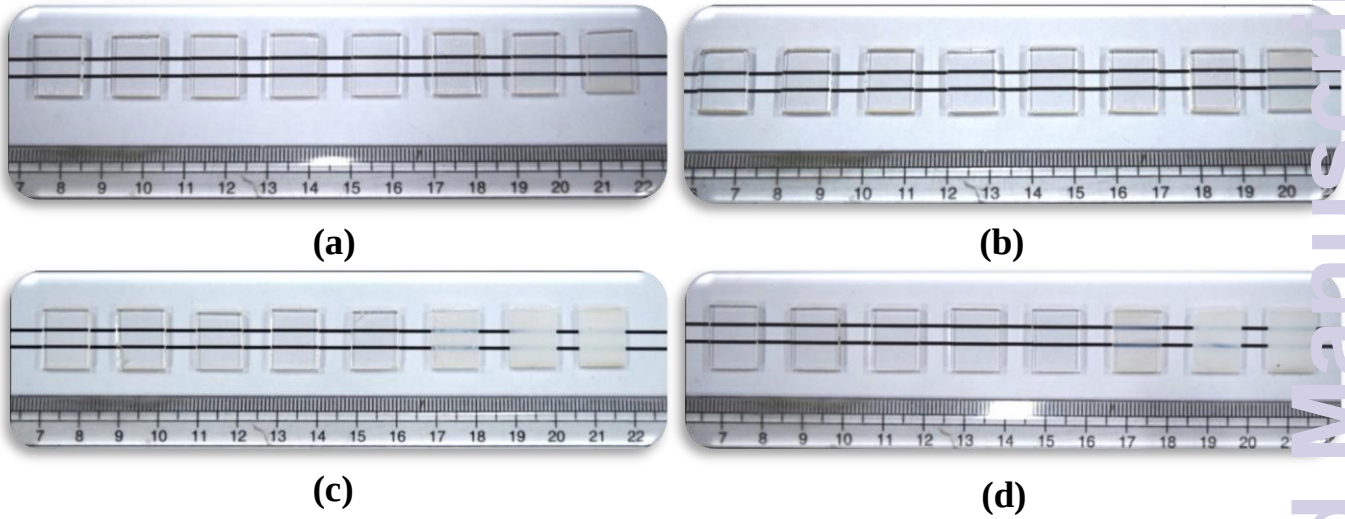

Fig 3. (Color online) Photograph of the heat treated samples of (a) CBS-1, (b) CBS-2, (c) CBS-3 and (d) CBS-4. Heat treatment is done at 650°C and the durations are (left to right) as prepared, 15m, 30m, 1h, 2h, 3h, 5h and 8h. The samples are laid down over black lines to show their transparency ((See Table 1 for composition).

View Article Online
DOI: 10.1039/C5RA15501K

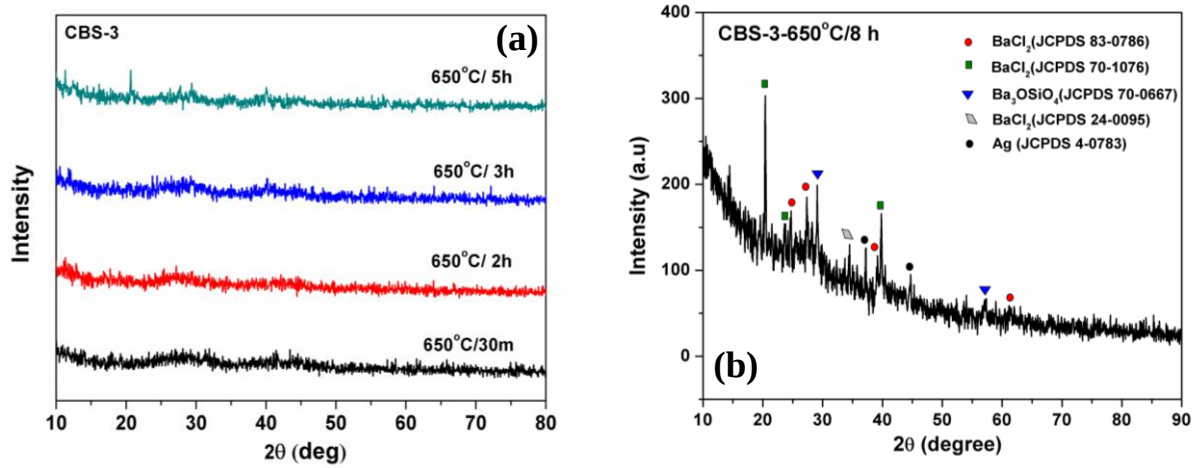

Fig 4. X-ray diffractogram of sample CBS-3 heat treated at 650°C for (a) 30m, 2h, 3h, 5h, (b) 8h, peaks have been identified with reference to corresponding JCPDS file numbers (See Table 1 for composition).

View Article Online
DOI: 10.1039/C5RA15501K

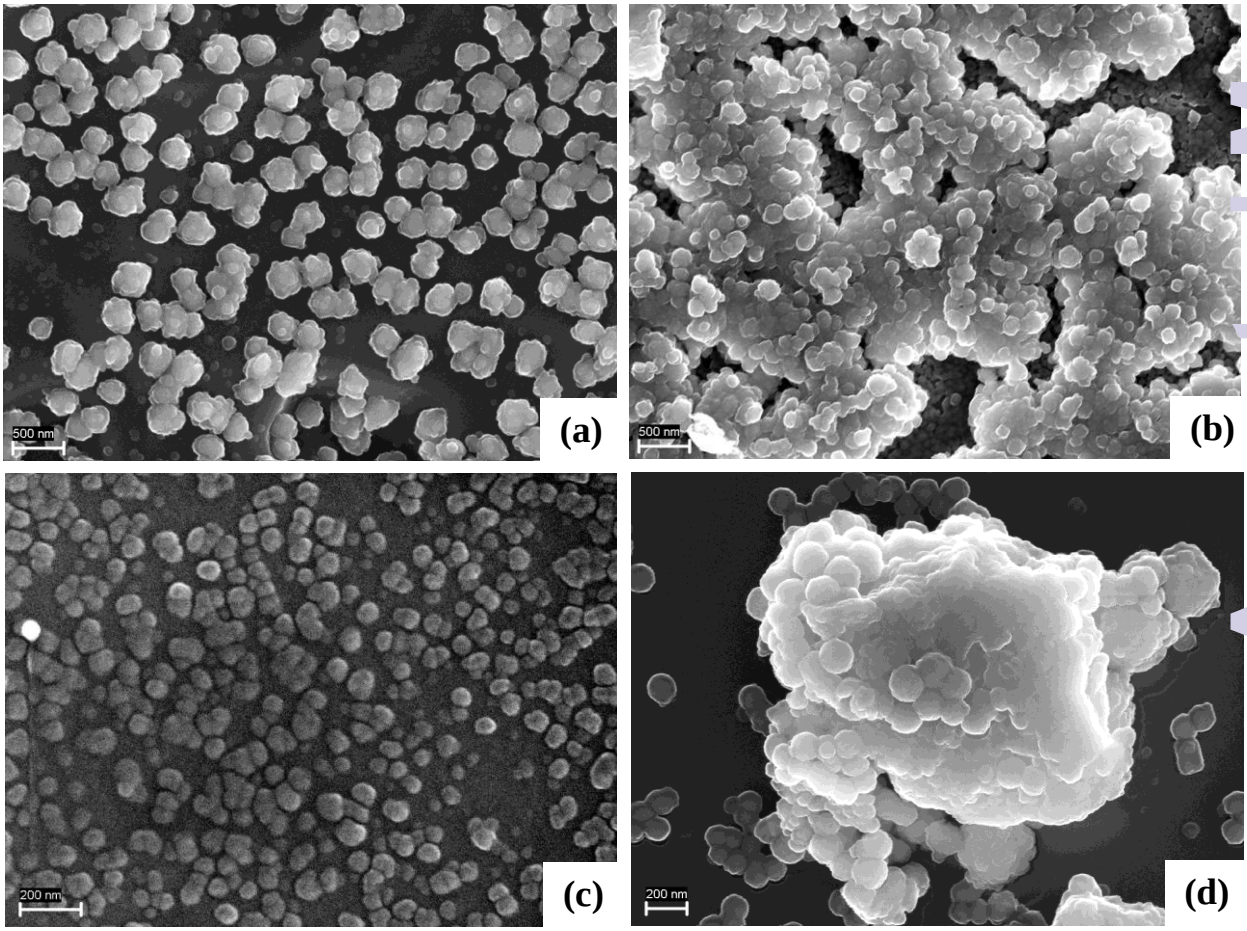

Fig 5. FESEM photo micrograph (a) and (b) of CBS-1, and (c) and (d) of CBS-3 heat treated at 650°C for 5h (See Table 1 for composition).

View Article Online
DOI: 10.1039/C5RA15501K

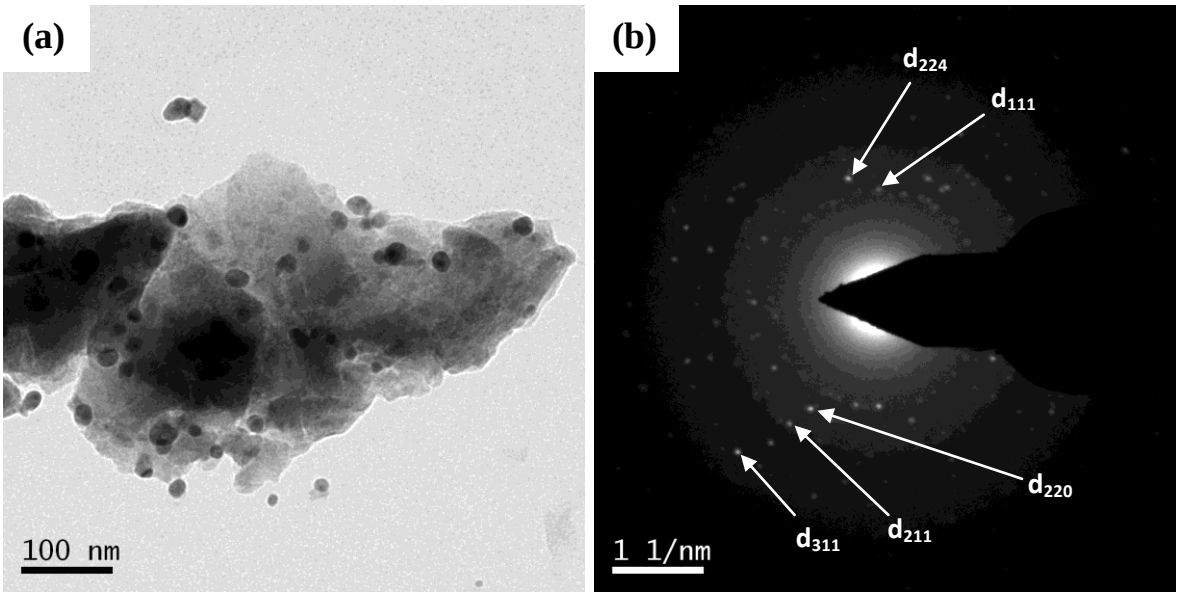

Fig 6. (a) TEM image and (b) SAED pattern of CBS-3 heat treated at 650°C for 5h (See Table 1 for composition).

View Article Online
DOI: 10.1039/C5RA15501K

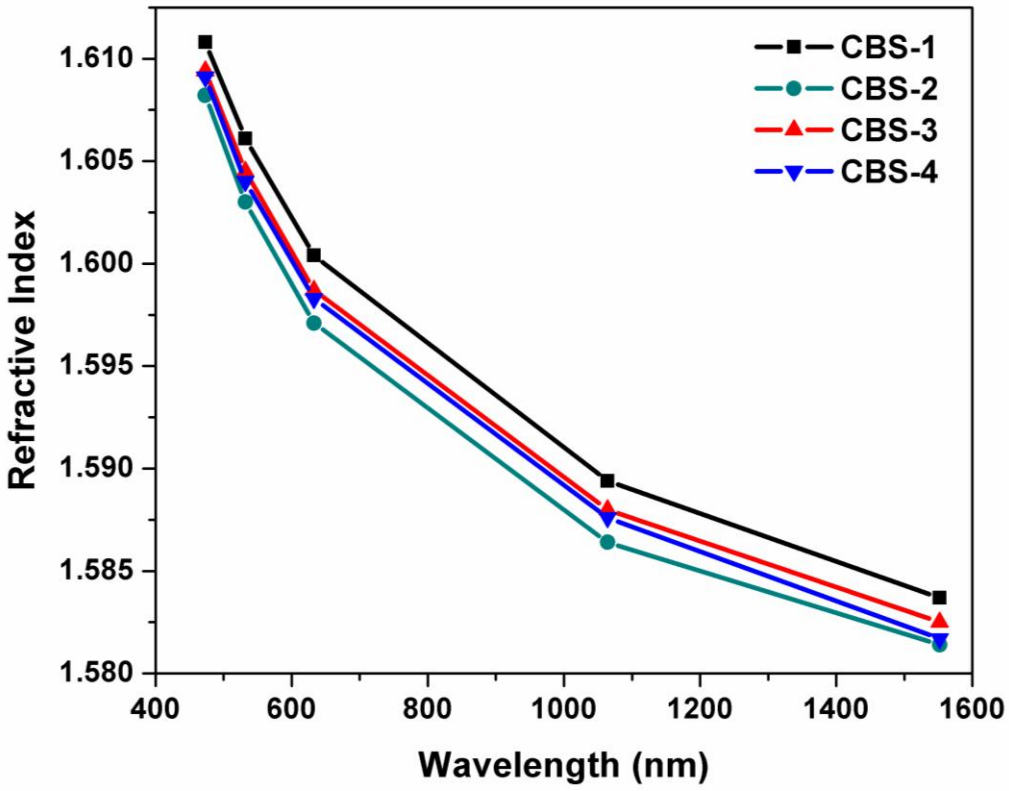

Fig 7. Refractive index of samples CBS-1, CBS-2, CBS-3 and CBS-4 as a function of wavelength (See Table 1 for composition).

View Article Online
DOI: 10.1039/C5RA15501K

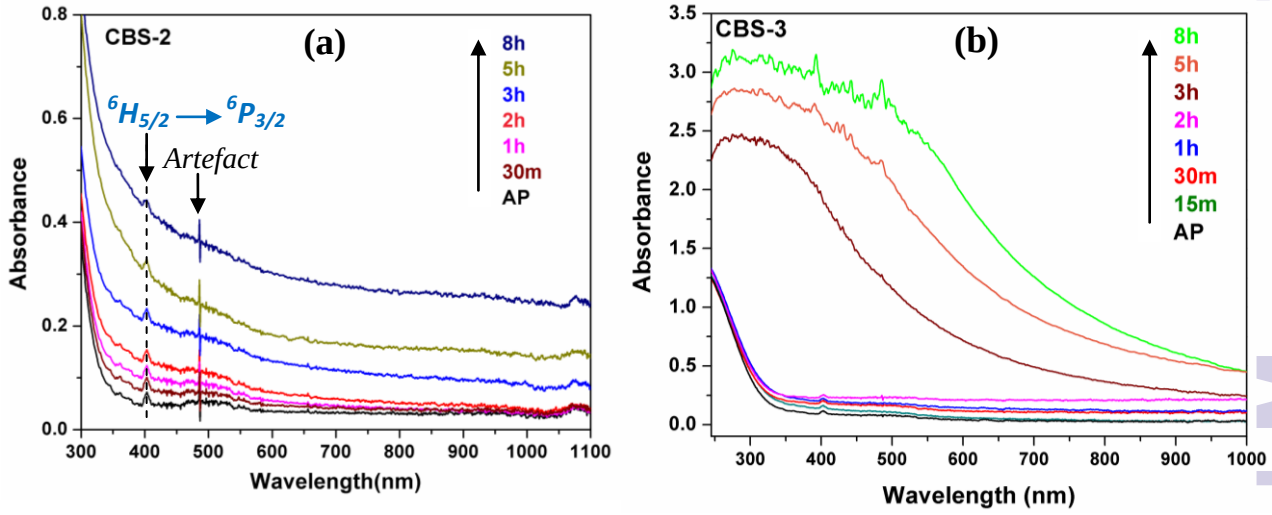

Fig 8. UV-Vis absorption spectra of (a) CBS-2 and (b) CBS-3 heat treated at 650°C for different durations (See Table 1 for composition).

View Article Online
DOI: 10.1039/C5RA15501K

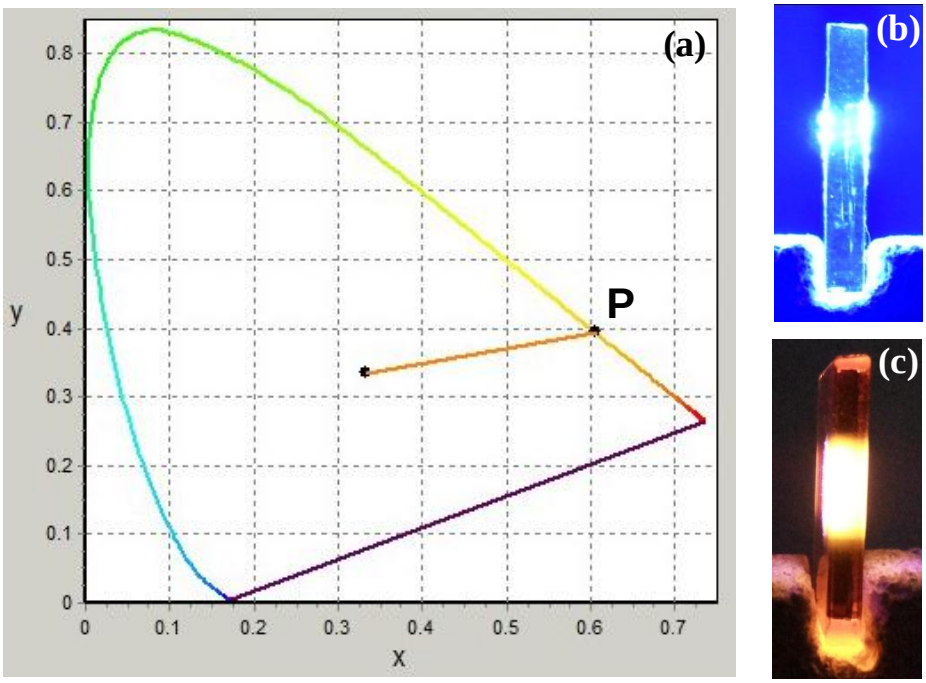

Fig 9. (a) Chromaticity diagram corresponding to the light emitted from CBS-3 heat treated at 650°C for 15m when excited at 446 nm with a diode laser source. The point "P" represents chromaticity coordinates (x=0.606, y=0.391) of the emitted light. Photoluminescence photographs of (b) CBS-1 and (c) CBS-3 heat treated at 650°C for 15m, when excited at 446 nm (See Table 1 for composition).

View Article Online
DOI: 10.1039/C5RA15501K

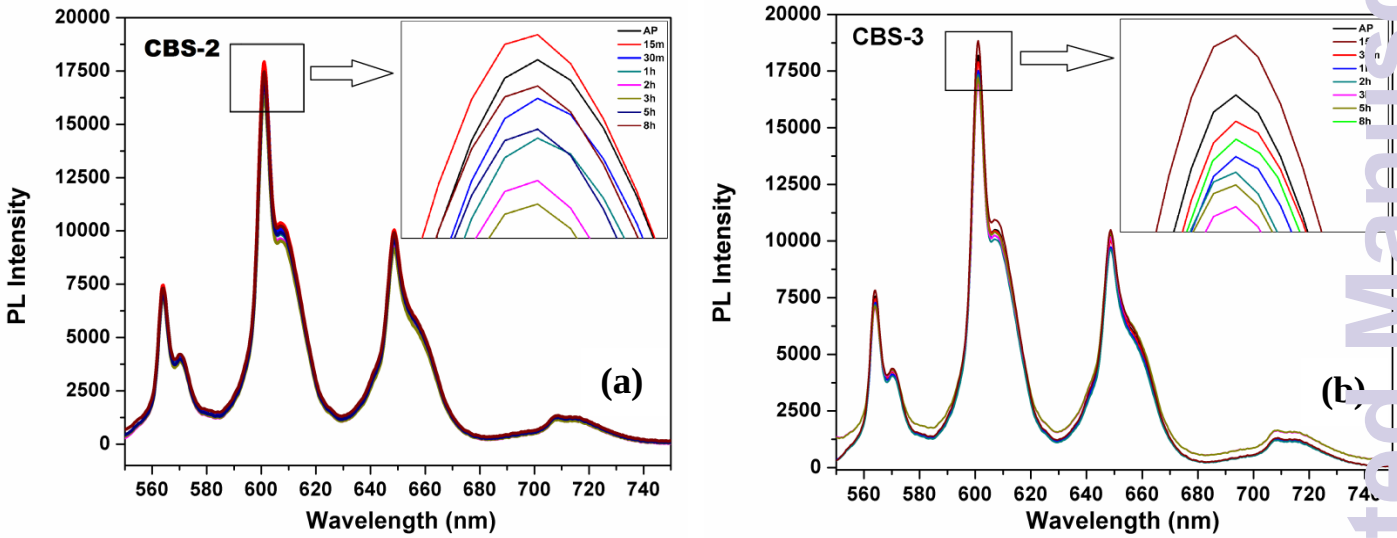

Fig 10. (Colour online) Photoluminescence spectra (excited at 446 nm) of (a) CBS-2 and (b) CBS-3 heat treated at 650°C for different durations (insets show the magnified view of the largest peak) (See Table 1 for composition).

View Article Online
DOI: 10.1039/C5RA15501K

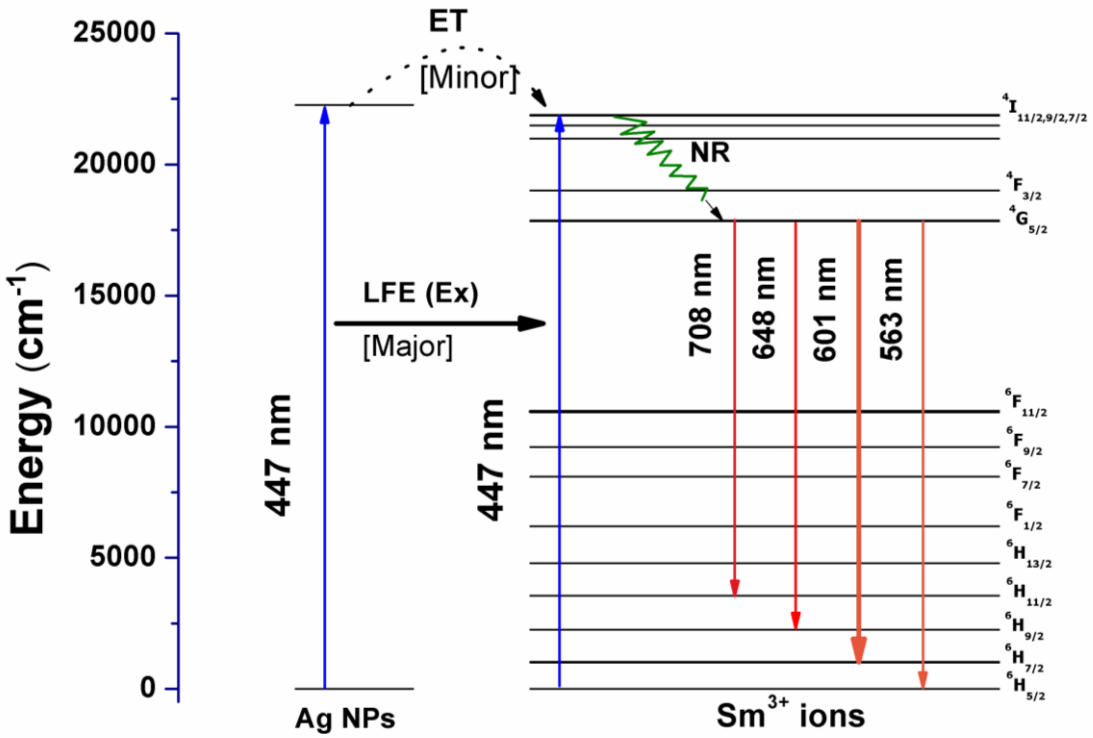

Fig 11. Partial energy level diagram of Sm^{3+} ion and Ag NPs showing the energy transfer mechanisms for the major bands in the downconversion spectra

View Article Online
DOI: 10.1039/C5RA15501K

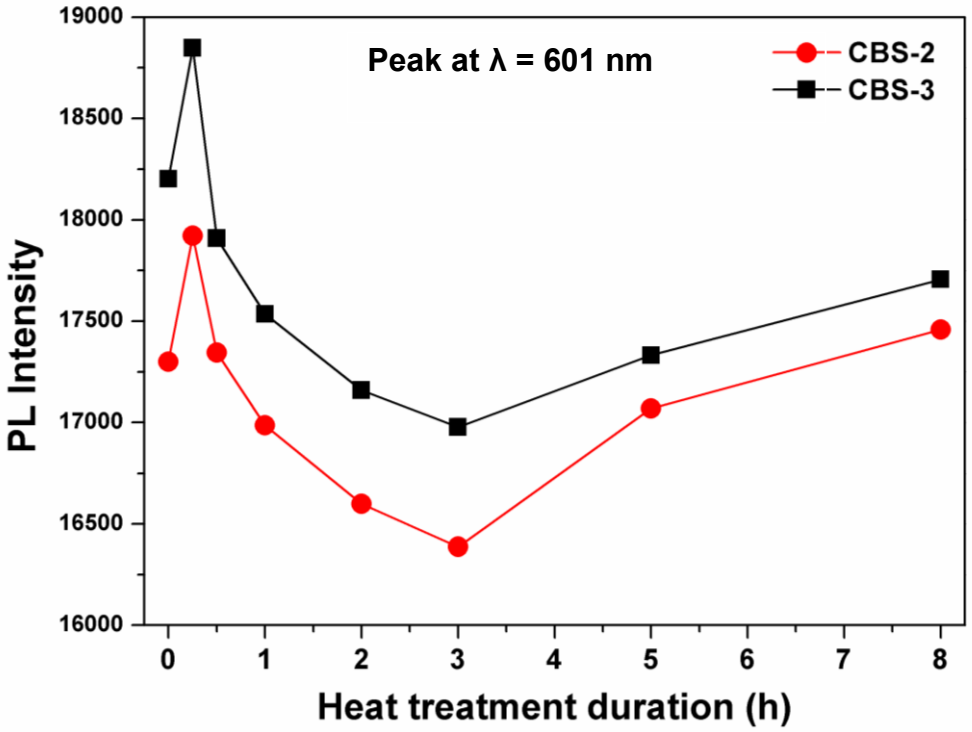

Fig 12. Variation of photoluminescence intensity of the emission peak at 601 nm of CBS-2 and CBS-3 as a function of heat treatment duration (See Table 1 for composition).

View Article Online
DOI: 10.1039/C5RA15501K

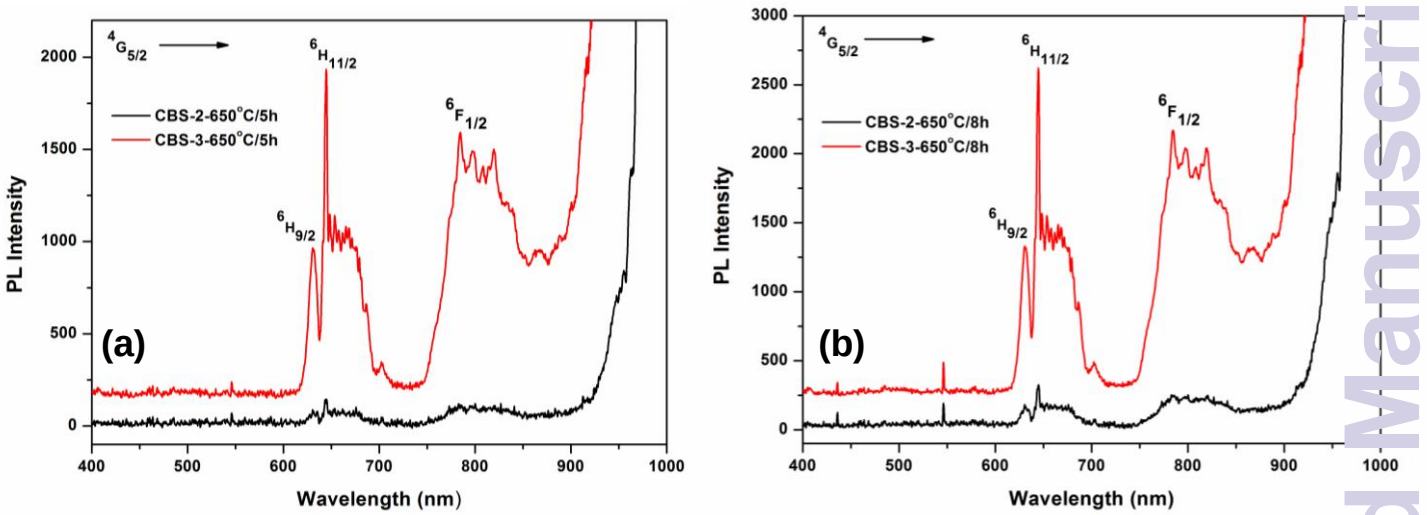

Fig 13. Photoluminescence spectra (excited at 980 nm) of (a) CBS-2 and (b) CBS-3 heat treated at 650°C for 5h and 8h (See Table 1 for composition).

View Article Online
DOI: 10.1039/C5RA15501K

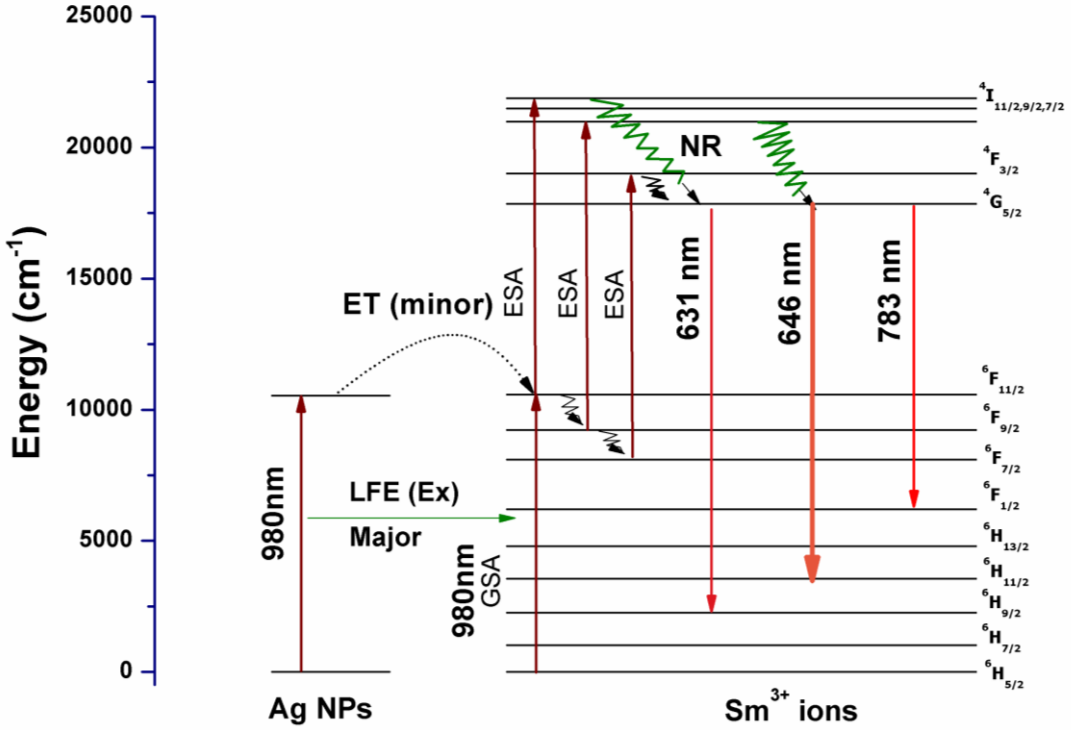

Fig 14. Partial energy level diagram of Sm^{3+} ion and Ag NPs showing the energy transfer mechanisms for the major bands in the upconversion spectra